Sensors and Actuators B 236 (2016) 781–793

Contents lists available at ScienceDirect

Sensors and Actuators B: Chemical

journal homepage: www.elsevier.com/locate/snb

In-situ electrosynthesized nanostructured Mn_3O_4-polyaniline nanofibers- biointerface for endocrine disrupting chemical detection

Nawab Singh [a], Md. Azahar Ali [b], Kali Suresh [c], Ved Varun Agrawal [d], Prabhakar Rai [e], Ashutosh Sharma [e,*], B.D. Malhotra [f,*], Renu John [a,*]

[a] Department of Biomedical Engineering, Indian Institute of Technology Hyderabad, Kandi, Sangareddy-502285 Telangana, India
[b] Department of Electrical and Computer Engineering, Iowa State University, Ames, IA-50011, USA
[c] Centre for Nanotechnology, Hyderabad Central University, Hyderabad Telangana-500046, India
[d] Centre on Biomolecular Electronics, Biomedical Instrumentation Section, CSIR-National Physical Laboratory, Dr. K. S. Krishnan Marg, New Delhi-110012, India
[e] Department of Chemical Engineering, Indian Institute of Technology Kanpur, Kanpur, 208016, India
[f] Department of Biotechnology, Delhi Technological University, Shahbad Daulatpur, Main Bawana Road, Delhi-110042, India

ARTICLE INFO

Article history:
Received 9 March 2016
Received in revised form 31 May 2016
Accepted 7 June 2016
Available online 8 June 2016

Keywords:
Nanofibers
Mn_3O_4 nanoparticles
Polyaniline
Bisphenol A
Tyrosinase

ABSTRACT

We report results of the studies relating to fabrication of an electrochemical biosensor platform based on *in-situ* electrosynthesized manganese oxide (Mn_3O_4)-polyaniline (PANI) nanofibers for detection of bisphenol A (BPA), an endocrine disrupting chemical. The spherical Mn_3O_4 nanoparticles synthesized using cetyltrimethylammoniumbromide were modified with PANI in presence of polyvinyl sulphonic acid and glutaraldehyde. The tyrosinase (Tyrs) molecules covalently immobilized on the PANI-modified Mn_3O_4 nanofibers surface were characterized using X-ray diffraction, electron microscopy and Fourier transform infrared spectroscopy. This electrochemical biosensor exhibits a response time of 20 s, sensitivity of 0.776 mA μM^{-1} L cm^{-2}, respectively, and 0.134 mA μM^{-1} L cm^{-2} in the concentration ranges, 0.004–0.09 $\times 10^{-6}$ mol L^{-1} and 0.2–0.8 $\times 10^{-6}$ mol L^{-1} of BPA.

1. Introduction

Polymeric materials are currently in increased demand in our daily lives due to their reusability, recoverability and stability [1]. Along with widespread applications of polymeric compounds in food, drinking water and packaging industry, questions have been posed on the harmfulness of these chemicals on human beings and animals. Bisphenol A (2, 2-bis (4-hydroxyphenyl) propane ($C_{15}H_{16}O_2$); BPA) is such a chemical that is used in manufacturing drinking water bottles, baby feeding bottles and food packaging industries [2]. It is also used for the synthesis of epoxy resins, polystyrene resins, polycarbonate, inner coating of food cans, dental sealants, food packaging and drug delivery systems [3]. BPA and other similar phenolic compounds are, therefore, a natural threat to our precious environment including drinking water. BPA is considered as an endocrine disrupting compound (EDC) since it may trigger secretion of natural estrogen by the human endocrine system, resulting in elevated estrogenic activity in the human body. EDCs are pollutants chemical that are known to affect the hormonal balance of various species including humans [4,5]. BPA has been reported to have adverse effects such as cancer [6], decreased semen quality, reduced immunity, heart diseases, obesity and impaired reproduction in human beings and animals [7–9]. Hence the detection of BPA in drinking water and food even at very low concentration is very crucial from a public health perspective. Several techniques such as high-performance liquid chromatography, gas chromatography, capillary electrophoresis, chemiluminescence, [2,10,11] and ELISA have been employed for the detection of BPA in a given environment. However, these methods are expensive, time consuming, and require special expertise for handling the complex procedure. Some immunosensors have been reported for detection of BPA using BIACORE 3000 sensor chip, [12] waveguide-based evanescent immunosensor, [13] and piezoelectric immunosensor [14]. In spite of these developments, there is enough scope for the development of an improved biosensing device that can be used for BPA detection.

Manganese oxide (Mn_3O_4) is one of the most stable transition metal oxides with a spinel structure. It is being explored for the development of rechargeable lithium ion batteries, catal-

* Corresponding authors.
E-mail addresses: ashutos@iitk.ac.in (A. Sharma), bansi.malhotra@gmail.com (B.D. Malhotra), renujohn@iith.ac.in, rjohniitd@gmail.com (R. John).

http://dx.doi.org/10.1016/j.snb.2016.06.050
0925-4005/

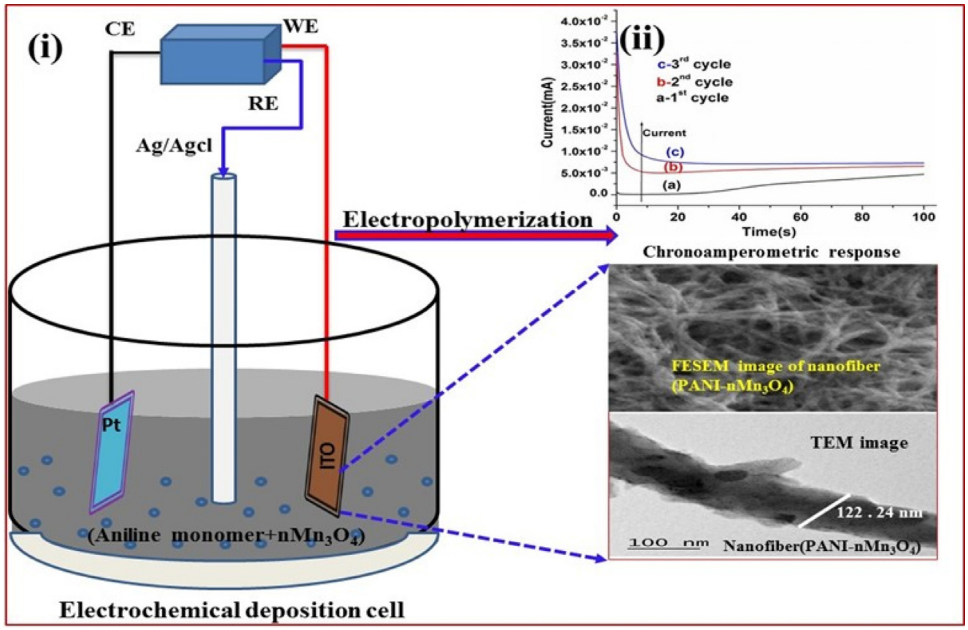

Fig. 1. (i) Schematic representation of In-situ electropolymerization of Mn_3O_4-polyaniline nanocomposite (ii) Chronoamperometric current responses during in-situ electropolymerization of Mn_3O_4 nanoparticles with aniline monomer.

ysis and molecular adsorption [15–17]. Mn_3O_4 is a tetragonal Hausmannite with Mn^{3+} and Mn^{2+} ions occupying octahedral and tetrahedral positions of the spinel structure, respectively. The octahedral symmetry of Mn_3O_4 is tetragonally distorted due to the Jahn–Teller effect on Mn^{3+} ions. The unit cell of Mn_3O_4 contains $Mn_4Mn_8O_{16}$ in which the oxygen atoms are closely packed with Mn^{2+} ion in tetrahedral-site and Mn^{3+} ion in octahedral-site [18,19]. The nMn_3O_4 exhibits ferrimagnetic behavior at Curie temperature (T_c = 40 K) and has excellent electron transport properties [20,21]. Due to excellent electron transfer, stability and electrochemical properties, nMn_3O_4 can perhaps be utilized for biosensing applications [22].

Polyaniline (PANI) is a conducting polymer that is known to be cost-effective, environmentally stable and has interesting tunable conducting properties. The composites of transition metal oxides and conducting polymers have been used for fabrication of supercapacitor electrodes [23,24]. The electrochemical polymerization has been utilized to prepare bioactive nanofiber (NF) of PANI-nMn_3O_4 in presence of aniline, polyvinyl sulphonic acid (PVSA) and hydrochloric acid. PANI-nMn_3O_4 NF is an attractive material that provides a suitable interface for immobilization of proteins due to large specific surface area, highly conductive nature and strong adsorption ability [25–28].

We report results of the studies relating to preparation of spherical nMn_3O_4 via co-precipitation method and electropolymerized with aniline in presence of hydrochloric acid (HCL) and polyvinylsulphonic acid (PVSA) as a binder using chronoamperometric technique. Glutraldehyde (GA) treatment was used to crosslink tyrosinase (Tyrs) with PANI-nMn_3O_4 electrode surface for detection of BPA using amperometric technique. We discuss the merits of this interesting nanohybrid biointerface for BPA detection.

2. Experimental

2.1. Chemicals and reagents

All chemicals used were of analytical grade. Manganese chloride, sodium hydroxide, cetyltrimethylammonium bromide (CTAB), aniline, HCL, PVSA, GA, tyrosinase (Tyrs), BPA, phenol, resorcinol, para-aminophenol, ortho-nitrophenol, and hydroquinone were purchased from Sigma Aldrich, USA. Deionized water used for all experiments was obtained from Millipore. Phosphate buffer saline (PBS) was prepared using sodium monohydrate phosphate (Na_2HPO_4) and sodium dihydrogen phosphate (NaH_2PO_4) reagents, following standard protocols.

2.2. Synthesis of nanostructured manganese oxide

Colloidal solution of Mn_3O_4 was prepared using manganese chloride ($MnCl_2$) as the precursor. 0.5 mol L^{-1} of $MnCl_2$ and 0.2 mol L^{-1} of NaOH were separately dissolved in 250 mL ethanol and distilled water, respectively and then mixed. Spherical nMn_3O_4 was synthesized by co-precipitation method by using cetyltrimethylammoniumbromide (0.4×10^{-3} mol L^{-1}) as a surfactant [29,30]. Thus formed precipitate was washed with deionized water and ethanol seven times and dried at 90 °C for 24 h, and then calcined at 450 °C for 4 h.

2.3. Fabrication of the sensor platform

2 mg of nMn_3O_4 was dispersed in 12 mL of 1 mol L^{-1} HCL by stirring constantly for 6 h and ultrasonicated for 90 min after which 100 μL of 0.1 mol L^{-1} distilled aniline was added. After 3 h of constant stirring in a dark place, 100 μL of 0.5 mol L^{-1} PVSA was added drop-wise while shaking. Subsequently, 10 mL of the solution was used for electropolymerization using chronoamperometric technique. The thin film of PANI-Mn_3O_4 is shown in [Fig. 1(i)]. The solution comprising of distilled aniline, PVSA and nMn_3O_4 dispensed in 1 mol L^{-1} HCL was used to prepare nanocomposite fibers via electropolymerization. During electrochemical deposition, the potential was kept at 1.5 V for three cycles of 100 s. After each cycle, electrode was washed with DI water drop-wise in order to form stable PANI-nMn_3O_4NF/ITO film and the current flowing through the electrode deposition was monitored for 100 s. The high current observed in the initial stage originated due to double layer charging. The stable electrochemical deposition current of PANI-nMn_3O_4 NF [Fig. 1 (ii-curve c)] during third cycle was found to be about 10 times higher compared to the second cycle (curve b) and the cur-

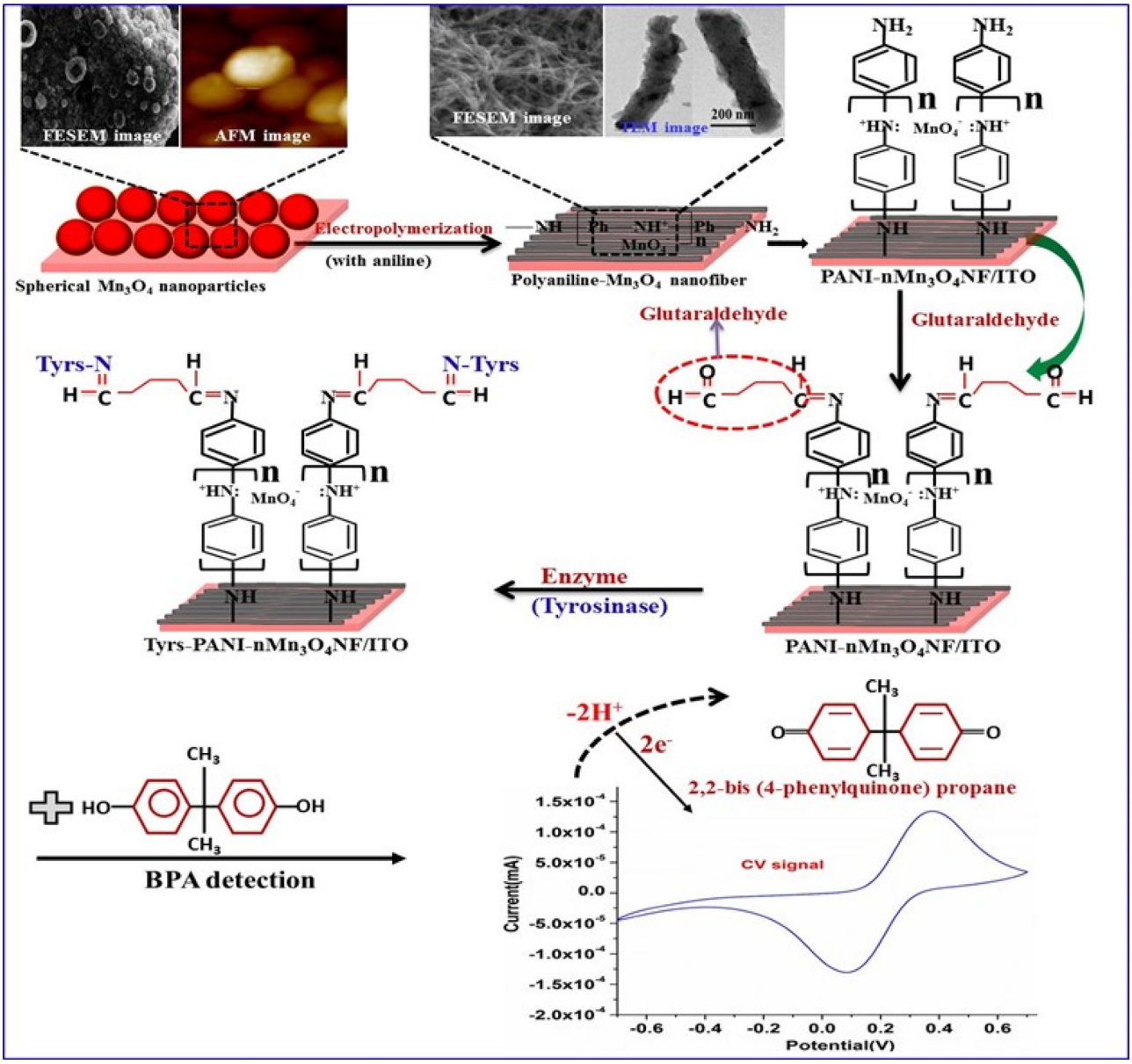

Fig. 2. Schematic representation of fabrication of a biosensor platform for detection of endocrine disrupting chemicals and the mechanism for crosslinking with enzyme molecules.

Table 1
Comparison table for various biosensors characteristics with the fabricated Tyrs-PANI-nMn_3O_4NF/ITO bioelectrode.

Electrodes	Techniques	Linear range (μM)	LOD (μM)	Sensitivity	Reference
Molecular Imprinted polymer film	EIS	0–12,000	420	0.00411 Ω mM^{-1} L	Apodaca et al. [37]
TyrsAPTES/nTiO_2/Ti	EIS	0.01–1.0	0.01	361.9 kΩ mM^{-1} L	Singh et al. [3]
Pt/Gr-CNTs	CV/DPV	0.06–10	0.042		Zheng et al. [31]
Polypyridyl ruthenium(II)	CV/DPV	5–120	0.29	0.22 μA $μM^{-1}$ L	Li et al. [38]
Tyrs MWNTs-CoPc-SF	CV	0.05–3.0	0.03		Yin et al. [39]
Tyrs/Thionine- carbon	CV	0.15–45	0.15	85.4 ± 1.5 nA $μM^{-1}$ L	Portaccio et al. [40]
MIP Au	CV	8–60	13.8	–	Huang et al. [41]
Tyrs@PANI-Mn_3O_4/ITO	CV	0.004–0.8	0.004	0.776 mA $μM^{-1}$ L cm^{-2}	Present Work

rent observed during the second cycle was about 20 times higher as compared to first cycle (curve a). It was found that the PANI-nMn_3O_4 NF could be uniformly deposited during the third cycle (curve c) after which PANI-nMn_3O_4 NF/ITO electrode was dipped in 1% GA for 2 h in a closed vessel for cross linking with enzyme (Tyrs) molecules. Fresh solution of Tyrs enzyme (0.2 unit/mL) was prepared in PBS (50×10^{-3} mol L^{-1}, pH 7.0) and was uniformly spread (10 μL) onto the PANI-nMn_3O_4 NF/ITO electrode surface and kept it in a humid chamber for 12 h at room temperature (27°C). The fabricated Tyrs immobilized PANI-nMn_3O_4NF/ITO bioelectrode was stored at 4 °C when not in use. The proposed mechanism for fabrication of Tyrs-PANI-nMn_3O_4NF/ITO bioelectrode and immobilization of Tyrs onto this electrode is shown in Fig. 2.

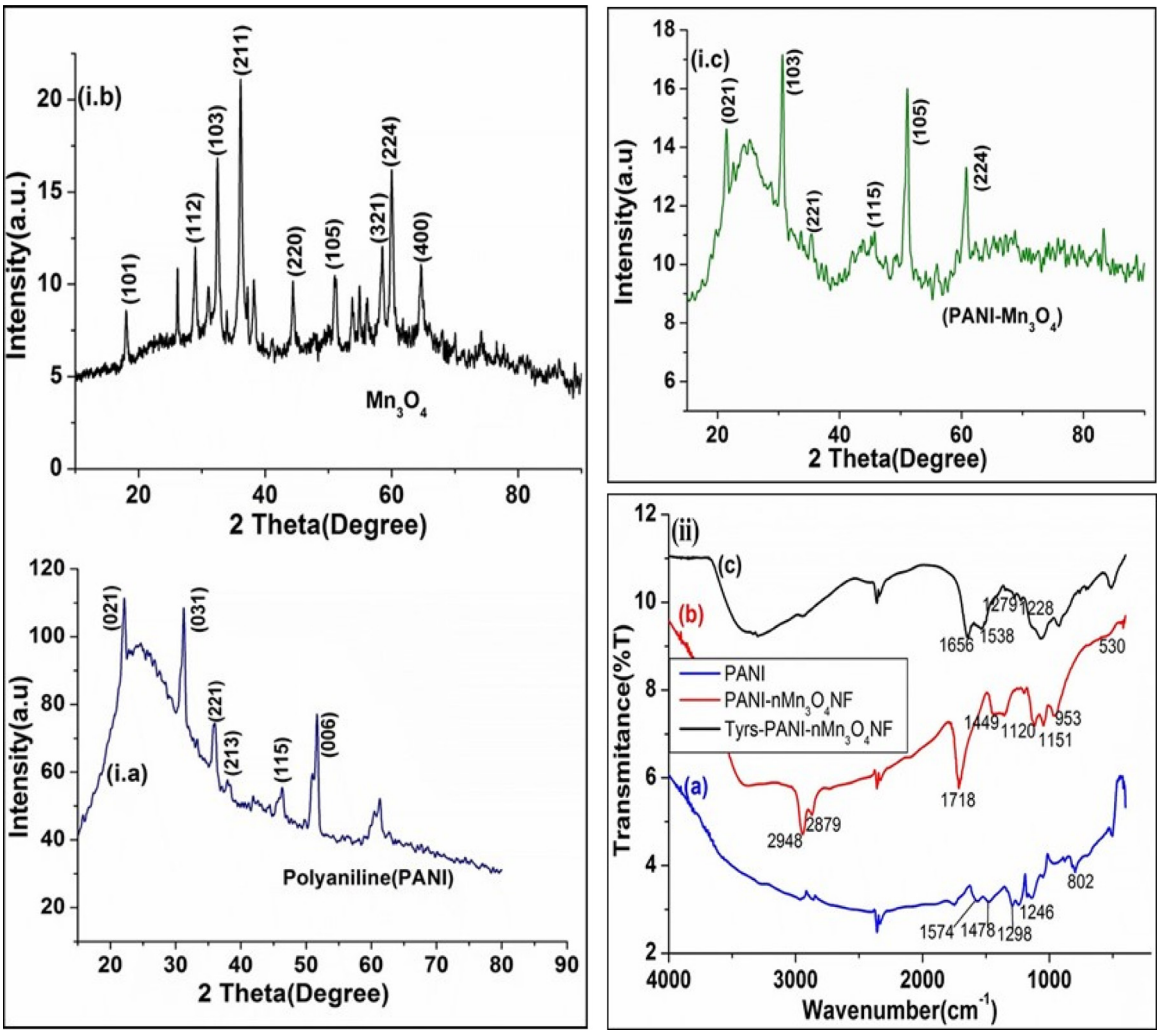

Fig. 3. (i) X-ray diffraction pattern of (i.a) polyaniline, (i.b) spherical Mn_3O_4 nanoparticle, and (i.c) PANI-nMn_3O_4 nanocomposite (ii) FTIR spectra of (a) polyaniline, (b) PANI-nMn_3O_4/ITO electrode and (c) Tyrs-PANI-nMn_3O_4/ITO bioelectrode.

2.4. Real sample preparation

A real sample solution of BPA was prepared using two types of plastic products (polyvinyl chloride and polycarbonate mineral water bottles) available in local market [3,31]. These plastic products were cut into small pieces and washed using double distilled water. Then 15.0 gm. plastic pieces were added into a 100 mL double distilled water and sealed. The solution was then ultrasonicated for 90 min at 60 °C, and kept at 85 °C with a water bath for 48 h. After filtration, the solution was collected in a flask. The extraction process was repeated three times, and the solutions were collected in the same flask and the concentration of the stock solution with BPA was found to be 0.520×10^{-6} mol L^{-1}. For dilution of this stock solution, we used deionized water with desired concentrations.

2.5. Characterization

Spherical nMn_3O_4 and its composite with PANI were characterized using X-ray diffraction (XRD, Rikagu) and high resolution transmission electron microscope (HRTEM, Jeol/JEM 2100). The surface morphology shapes were studied using field emission scanning electron microscope (FESEM, ZEISS) and atomic force microscope (AFM, BRUKER NanoScope®.V-4498BE). The elemental analysis was conducted using energy dispersive X-ray spectroscopy (EDAX). Fourier transform infra-red spectroscopy (FT-IR) from Perkin Elmer, (Spectrum BX II) was used for confirmation of the functional groups in Tyrs enzyme immobilized on electrode surface. X-ray photoelectron spectroscopy (XPS; PHI 5000 Versa Prob II, FEI Inc.) studies have conducted to investigate the functional groups and chemical bonding of the synthesized materials. Electrochemical studies were performed using Autolab Potentiostat/Galvanostat (Metrohm, Netherlands) in a three-electrode system with PANI-nMn_3O_4 deposited on indium tin oxide (ITO) glass substrate as a working electrode, platinum (Pt) as the auxiliary electrode and Ag/AgCl as reference electrode in phosphate buffer saline (PBS) (50×10^{-3} mol L^{-1}, pH 7.4, 0.9% NaCl) containing 5×10^{-3} mol L^{-1} $[Fe(CN)_6]^{3-/4-}$ as mediator.

3. Results and discussion

3.1. Structural properties

Fig. 3.i (a–c) shows the X-ray diffraction (XRD) pattern obtained for PANI, nMn_3O_4, and PANI–nMn_3O_4 nanocomposite. The XRD pattern of PANI film [Fig. 3 (i.a)] shows peaks at $2\theta = 22.07$, 31.16, 35.70, 37.98, 46.22, and 51.65 that correspond to (0 2 1), (0 3 1), (2 2 1), (2 1 3), (1 1 5), and (0 0 6) reflection planes, respectively. These are well-matched with JCPDS file 53-1891. This indicates that PANI film is semi-crystalline [32] and the structure is orthorhombic with cell parameters a = 6.98, b = 8.63, c = 10.44 with respect to α,

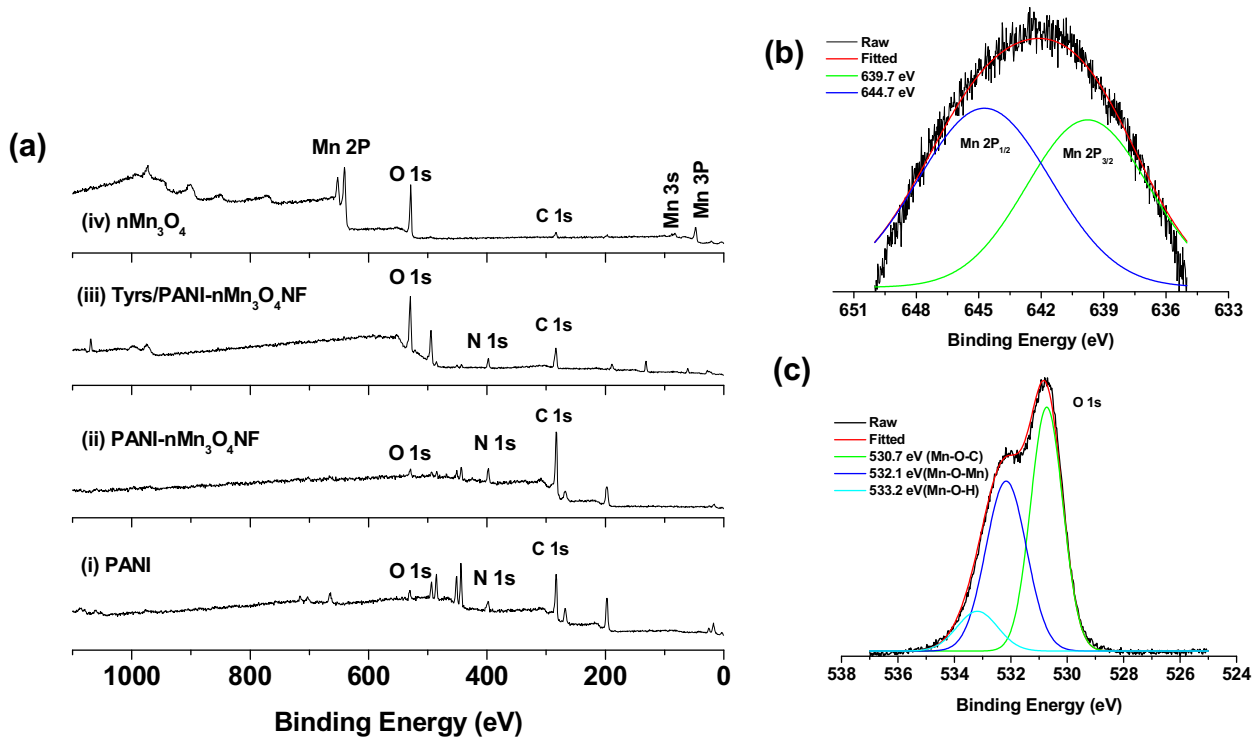

Fig. 4. (a) Wide-scan spectra for various fabricated films in the energy region of 0–1100 eV. (b) The XPS core-level spectra of Mn 2 P and (c) core-level spectra of O 1 s for Mn_3O_4 film.

β, γ, respectively. The additional peaks found in the XRD spectra are ascribed to the ITO substrate. The presence of dominant peaks of nMn_3O_4 in the XRD pattern for synthesized spherical nMn_3O_4 [Fig. 3 (i.b)] reveals high degree of crystallinity as well as purity of the sample. The diffraction peaks seen at 2θ = 18.11, 28.84, 32.50, 36.15, 44.44, 51.07, 58.37, 60.02, and 64.60 pertain to (1 0 1), (1 1 2), (1 0 3), (2 1 1), (2 2 0), (1 0 5), (3 2 1), (2 2 4), and (4 0 0) reflection planes, respectively, are well matched to the tetragonal spinel structure of Mn_3O_4. These results are consistent with the values obtained for Mn_3O_4 (JCPDS files, 89-4837, 80-0382 and 24-0734). The average crystallite size of nMn_3O_4 obtained by Debye–Scherrer equation is found to be 25–28 nm for the 2 1 1 plane. The nMn_3O_4 has a tetragonal Hausmanite structure with body centered lattice parameters as a = 5.76 A°, c = 9.44 A° with respect to α, and γ, respectively, which are in agreement with JCPDS 24-0734. The XRD spectra of PANI–nMn_3O_4 nanocomposite [Fig. 3(i.c)] shows diffraction peaks at 2θ = 21.45°, 31.04°, 35.37°, 45.88°, 51°, and 60.60° corresponding to (0 2 1) (1 0 3), (2 2 1) (1 1 5), (1 0 5), and (2 2 4) reflection planes of the tetragonal phase of nMn_3O_4, respectively. The crystallite size for PANI–nMn_3O_4 nanocomposite is found to be 30–35 nm for the (1 0 3) plane. The selected area electron diffraction (SEAD) indicates crystallinity in PANI–nMn_3O_4 nanocomposite with improved charge transfer properties of the electrochemical biosensor [inset, Fig. 4 (iii)]. The results indicate that the nMn_3O_4 interact with the anilinium cation and oligomers, that are formed during the initial stage of the polymerization and act as a template for the self-assembly of the PANI chains in a well-ordered manner.

Fig. 3 (ii) shows the Fourier transform infra-red (FT-IR) spectra of PANI, PANI-nMn_3O_4 NF, and Tyrs-PANI-nMn_3O_4 NF films. The FT-IR spectrum of bare PANI (curve a) shows characteristic vibrational peaks at 1574, 1478, 1298, 1246, and 804 cm^{-1}. The peaks found at 1574 and 1478 cm^{-1} are attributed to the C=C quinoid ring stretching vibrations and benzenoid structure of PANI, respectively. The characteristic peak pertaining to PANI backbone is observed at 804 cm^{-1}. The peaks found at 1298 and 1246 cm^{-1} correspond to the C—N and —C=N stretching vibrations due to emeraldine salt in PANI indicating that aniline is polymerized at the surface of ITO electrode with free $—NH_2$ groups [25]. The FTIR spectra of PANI-nMn_3O_4 NF shown in (curve b) exhibits additional peaks at 1718 cm^{-1} and 1449 cm^{-1} due to carbonyl (C=O) stretching of aldehyde and C—C stretching of the aromatic ring, respectively. The peaks observed at 2948 and 2879 cm^{-1} are attributed to the stretching of –C—H bond. The FTIR spectra obtained for the nanocomposite shows similar characteristic peaks. However, the peaks for bare PANI film are found to be shifted due to the formation of hydrogen bonding between Mn_3O_4 and the –NH groups of PANI. In addition, the nanocomposite exhibits characteristic peaks at 953 and 530 cm^{-1} in the fingerprint region arising due to the vibrations of Mn–O are associated with the coupling between Mn–O stretching modes of tetrahedral and octahedral sites [33]. After immobilization of Tyrs on the surface of PANI-nMn_3O_4 NF (curve c), the peaks observed at 1228 cm^{-1} and 1279 cm^{-1} correspond to —C=N stretching vibrations of the amide. The peaks seen at 1539 cm^{-1} and 1656 cm^{-1} are attributed to the NH bending in carbonyl amide bond. These results confirm the surface functionalization of PANI-nMn_3O_4 NF with Tyrs enzyme.

The X-ray photoelectron spectroscopy (XPS) studies were undertaken to confirm the presence of the functional groups in nMn_3O_4, PANI NF, PANI-nMn_3O_4 NF and Tyrs-PANI-nMn_3O_4NF films on ITO electrode and the formation of amide between enzymes and PANI-nMn_3O_4 NF electrodes. The C 1s, N 1s, and O 1 s peaks in the wide-scan spectrum of PANI NF, PANI-nMn_3O_4 NF and Tyrs-PANI-nMn_3O_4NF films are shown in Fig. 4 (i–iii). The Mn 2P, Mn 3P, Mn 3s, and O 1 s peaks found in the wide-scan spectra of nMn_3O_4 indicate the formation of nMn_3O_4 Fig. 4 (iv). All core-level spectra were deconvoluted into characteristic peaks using a Shirley baseline with a Gaussian profile. The Mn 2 P peak for nMn_3O_4 film was deconvoluted and split into two characteristic peaks at binding energies of 639.7 ($Mn2P_{3/2}$) and 644.4 eV ($Mn2P_{1/2}$) due to occurrence of Mn^{4+} (Fig. 4b). The O 1 s peaks for nMn_3O_4 film at 530.7,

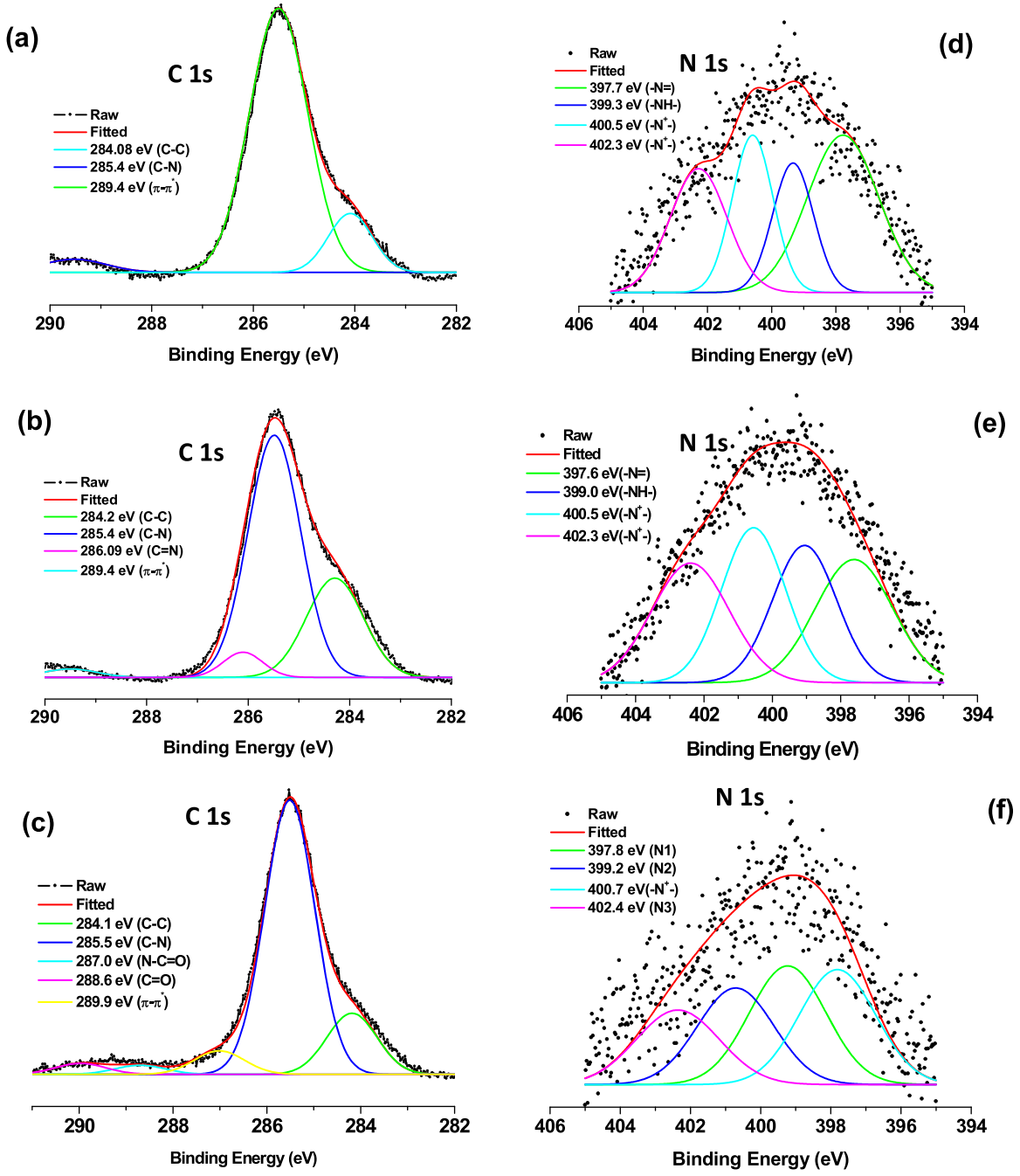

Fig. 5. XPS core-level spectra of C 1 s for the PANI NF (a), PANI-nMn_3O_4 NF (b) and Tyrs/PANI-nMn_3O_4 NF (c) electrodes. Core-level spectra of N 1 s for the PANI NF (a), PANI-nMn_3O_4 NF (b) and Tyrs/PANI-nMn_3O_4 NF (c) electrodes.

532.1 and 533.2 eV correspond to Mn—O—C, Mn—O—Mn and Mn-O—H, respectively and are due to the formation of metal–O—C bond, and metal-O (Fig. 4c).

The XPS C 1 s peaks found at 284.08, 285.4, and 289.4 eV pertain to the PANI NF electrode alone, without nMn_3O_4 and Tyrs enzyme, due to the C—C group in the aromatic ring, C—N bonds, and the p–p* "shake-up" satellite, respectively (Fig. 5a, top graph). On incorporation on nMn_3O_4 into PANI electrode, no significant changes of these C 1 s peaks were observed. However, one additional peak at binding energy of 286.09 eV corresponds to the C=N bond present in the composite formation and the peak due to the C—C groups in PANI is shifted to higher binding energy of 0.2 eV (Fig. 5b). After Tyrs immobilization onto PANI-nMn_3O_4 NF, the additional peaks found at binding energies of 287.0 and 288.6 eV, correspond to N—C=O and C=O bonds due to covalent amide bond formation between Tyrs enzyme and PANI-nMn_3O_4 in presence of glutaraldehyde cross-linker (Fig. 5c). Fig. 3d shows the N 1 s core-level spectra for PANI NF without nMn_3O_4 and Tyrs enzyme. The peaks for N 1 s core level of PANI at the binding energies of 397.7, 399.3, and 400.5 eV are due to presence of —N=, –NH-, and —N^+-, respectively in PANI matrix (Fig. 5d). These peaks with modification of nMn_3O_4 in PANI matrix were not significantly shifted (Fig. 5e). After enzyme immobilization, the peak found at 297.9 eV correspond to the core-level electrons of N 1 s (N1), the peak at 399.2 eV is due to amide bond (CO—NH) formation (N2), and the peak at 402.4 eV is assigned to presence of ≡N species in enzymes (N3) (Fig. 5f). However, the peaks at binding energies of 297.9 eV and 399.2 eV for N 1 s pertaining to enzymes and PANI are perhaps overlapped. These results

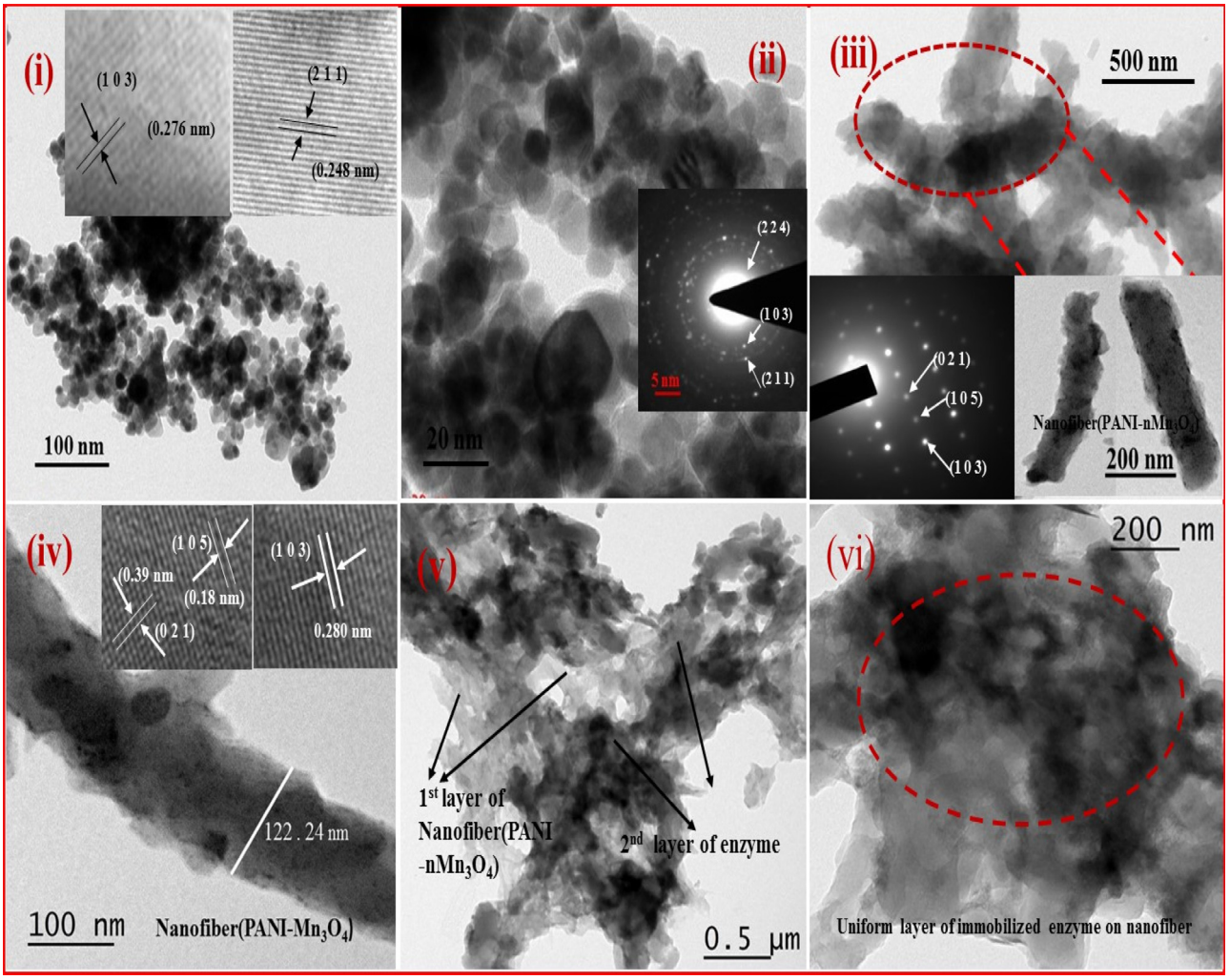

Fig. 6. (i and ii) TEM images of spherical Mn_3O_4 nanoparticles, inset images are HRTEM and SAED pattern, (iii and iv) TEM images of PANI-nMn_3O_4 nanofibers, inset zoom image of PANI-nMn_3O_4 nanofiber, inset images are HRTEM and SAED pattern, (v and vi) TEM images of Tyrs-PANI-nMn_3O_4/ITO bioelectrode after Tyrs immobilization.

confirm the formation of composite and covalent immobilization with Tyrs enzyme molecules.

To investigate the size of the synthesized nMn_3O_4 and PANI NF modified with nMn_3O_4, we conducted high resolution-transmission electron microscopy (HR-TEM). It is found that the nanostructure contains uniformly sized fine granules [Fig. 6(i-ii)] of nMn_3O_4 with hexagonal shape (20–25 nm). The clear lattice fringes seen in SAED pattern [inset, Fig. 6(ii)] indicate highly crystalline structure of the nMn_3O_4. In the atomic scale image (i, inset), two different lattice spacings (d) for (2 1 1) and (1 0 3) planes obtained are 0.248 nm and 0.276 nm, respectively. These results are in support of the JCPDS files 24-0734 and 80-0382, respectively indicating that growth of the nanoparticles occurs mostly along the 2 1 1 and 1 0 3 directions. After electropolymerization with aniline, the PANI coated nMn_3O_4 nanocomposite shows NF network [Fig. 6(iii–iv)]. A single PANI coated nMn_3O_4 NF of about 122.24 nm diameter is shown in image (iv). The SAED pattern of PANI-nMn_3O_4 nanocomposite indicates existence of the (1 0 3), (1 0 5) and (0 2 1) planes (inset, iii) that exactly match with the lattice spacing with d values of 0.280 nm, 0.18 nm and 0.39 nm, respectively (inset in Fig. 6(iv)). These results reveal that electropolymerized PANI-nMn_3O_4 NF provides a suitable biointerface for uniform linking of the Tyrs biomolecules. And it can be seen that Tyrs enzyme is uniformly attached with PANI-nMn_3O_4 NF surface due to inter-particle interactions of PANI-nMn_3O_4 NF and Tyrs enzyme molecules via GA [image (v–vi)].

3.2. Surface morphological studies

The SEM image [Fig. 7(i)] shows that the nMn_3O_4 are closely packed, and porous. The nMn_3O_4 exhibits numerous flower-like aggregations [inset in Fig. 7(i)] and some are elongated in structure. To investigate the atomic ratio and weight% of Mn and O, we carried out elemental (EDAX) analysis for the synthesized nMn_3O_4 [Fig. 7(ii)]. This study confirms the presence of 35 wt% of O and 65 wt% of Mn in the spherical nMn_3O_4 indicating high concentration of manganese and oxygen elements. The EDAX mapping for nMn_3O_4 after calcination containing mixed elements of Mn and O is shown in Fig. S1(a). The EDAX mapping confirms the presence of Mn (image b, Fig. S1) and oxygen elements (image c, Fig. S1) in Mn_3O_4 nanoparticles. It appears that most nanoparticles have spherical flower-like microsphere morphology, with globular 3D structure [Fig. 7 (iii) and (iv)]. After electropolymerization of nMn_3O_4 with PANI on ITO, a fibrous film of PANI-coated nMn_3O_4 is obtained [Fig. 7(v)]. The electropolymerized PANI-nMn_3O_4 results in the formation of symmetrical fibers of PANI-coated nMn_3O_4 deposited on the ITO substrate. The porous surface morphology of nanofibrous PANI-nMn_3O_4 is beneficial for immobilization of Tyrs enzyme molecules. Further, the PANI-nMn_3O_4NF/ITO surface

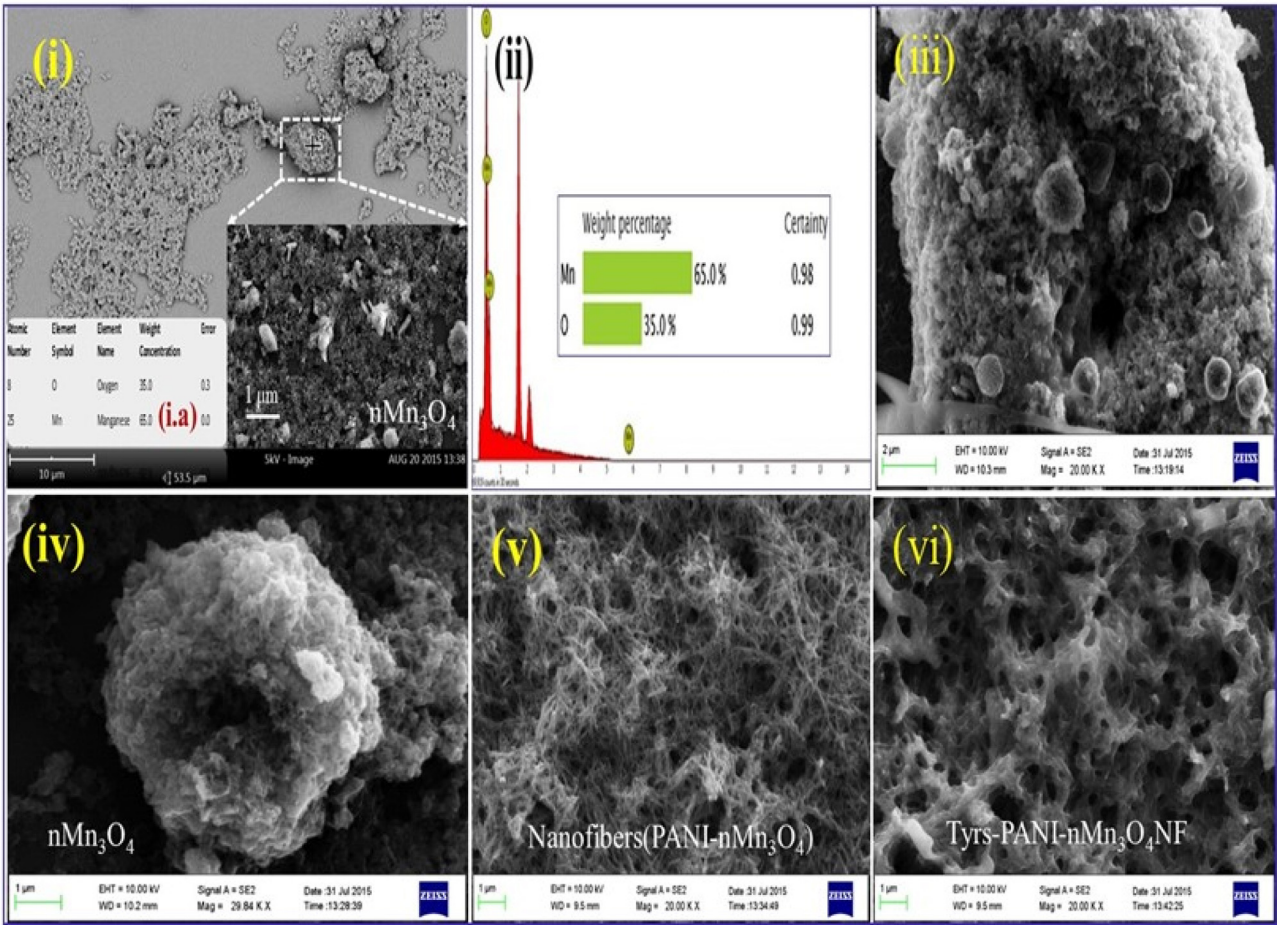

Fig. 7. (i) SEM image of spherical Mn_3O_4 nanoparticles, inset shows magnified image of spherical Mn_3O_4 nanoparticles, (ii) Elemental analysis (EDAX) image of spherical Mn_3O_4 nanoparticles, (iii and iv) FESEM images of spherical Mn_3O_4 nanoparticles, (v) FESEM image of PANI-nMn_3O_4 nanofibers, and (vi) FESEM image of Tyrs-PANI-nMn_3O_4/ITO bioelectrode after Tyrs immobilization.

was functionalized with GA via amino groups of the polyaniline surface for binding of the enzyme molecules.After enzyme immobilization, the change in morphology of Tyrs-PANI-nMn_3O_4NF/ITO surface perhaps occurred [Fig. 7(vi)] due to the covalent interaction of GA and enzyme. The FESEM image of enzyme immobilized on PANI-nMn_3O_4 NF shows a well- arranged and uniform fiber network, that further confirms strong enzyme binding.

The micrograph [Fig. S2 (i)] shows partially uniform spherical nMn_3O_4. The average size of the spherical nMn_3O_4 is calculated as 104 nm with average film roughness of 22.7 nm. The magnified image of nMn_3O_4 and the 3D image are shown in the inset of [Fig. S2 (i.a) and (vi)], respectively. After electropolymerization of PANI-nMn_3O_4 (image ii and iii), the changes in the grain size distribution, structural arrangement and shape of the PANI-nMn_3O_4NF/ITO are observed. The average roughness of PANI-nMn_3O_4NF/ITO film is found to be 90.7 nm. [Fig. S2 (iv)] and its 3D image (v) shows immobilization of the Tyrs enzyme onto the surface of PANI-nMn_3O_4NF/ITO. The Tyrs-PANI-nMn_3O_4NF/ITO electrode surface becomes uneven with increased value of average roughness (331 nm) indicating that Tyrs is adsorbed onto the PANI-nMn_3O_4NF/ITO surface.

3.3. Electrochemical studies

The electrochemical impedance can be represented as the sum of the real (Z′) and imaginary (Z″) components that mainly originate from the resistance and capacitance of an electrochemical cell. Fig. 8(i) shows the EIS spectra of various electrodes obtained as a function of frequency (0.01–105 Hz) at a bias potential of 0.01 V and the equivalent circuit for the EIS measurements [inset in Fig. 8 (i)]. The charge transfer resistance (R_{CT}) between the electrolyte and electrode can be described by (Eq. (1)), [34]

$$Z(\omega) = R_s + \frac{R_{CT} + \sigma\omega^{-1/2}}{\left(C_d\sigma\omega^{1/2}+1\right)^2 + \omega^2 C_d^2\left(R_{CT}+\sigma\omega^{-1/2}\right)2} - j\frac{\omega C_d\left(R_{CT}+\sigma\omega^{-1/2}\right)2 + \sigma\omega^{-1/2}\left(\sigma\omega^{1/2}C_d+1\right)}{\left(C_d\sigma\omega^{1/2}+1\right)^2 + \omega^2 C_d^2\left(R_{CT}+\sigma\omega^{-1/2}\right)2} \quad (1)$$

where R_s is the solution resistance, C_d is the double layer capacitance, ω is the 2πf, where f is the frequency, and σ is defined by

$$\sigma = \frac{RT}{\sqrt{2}F^2A}\left(\frac{1}{\sqrt{D_o}C_o^*} + \frac{1}{\sqrt{D_R}C_R^*}\right)$$

where A is the area of the electrode, D_o and D_R are respectively the diffusion coefficients of oxidant and reductant, C_o^* and C_R^* are the bulk concentrations of oxidant and reductant, respectively, and other symbols have the standard meanings. The R_{CT} value can be calculated from semicircular region in the Nyquist plot and it is found to be lower (551.4 Ω, curve b) for PANI-nMn_3O_4NF/ITO electrode compared to that of the bare ITO electrode (1.94 kΩ, curve a). This is due to the formation of PANI-nMn_3O_4 NF that provides excellent electrical contact between the PANI-nMn_3O_4NF/ITO elec-

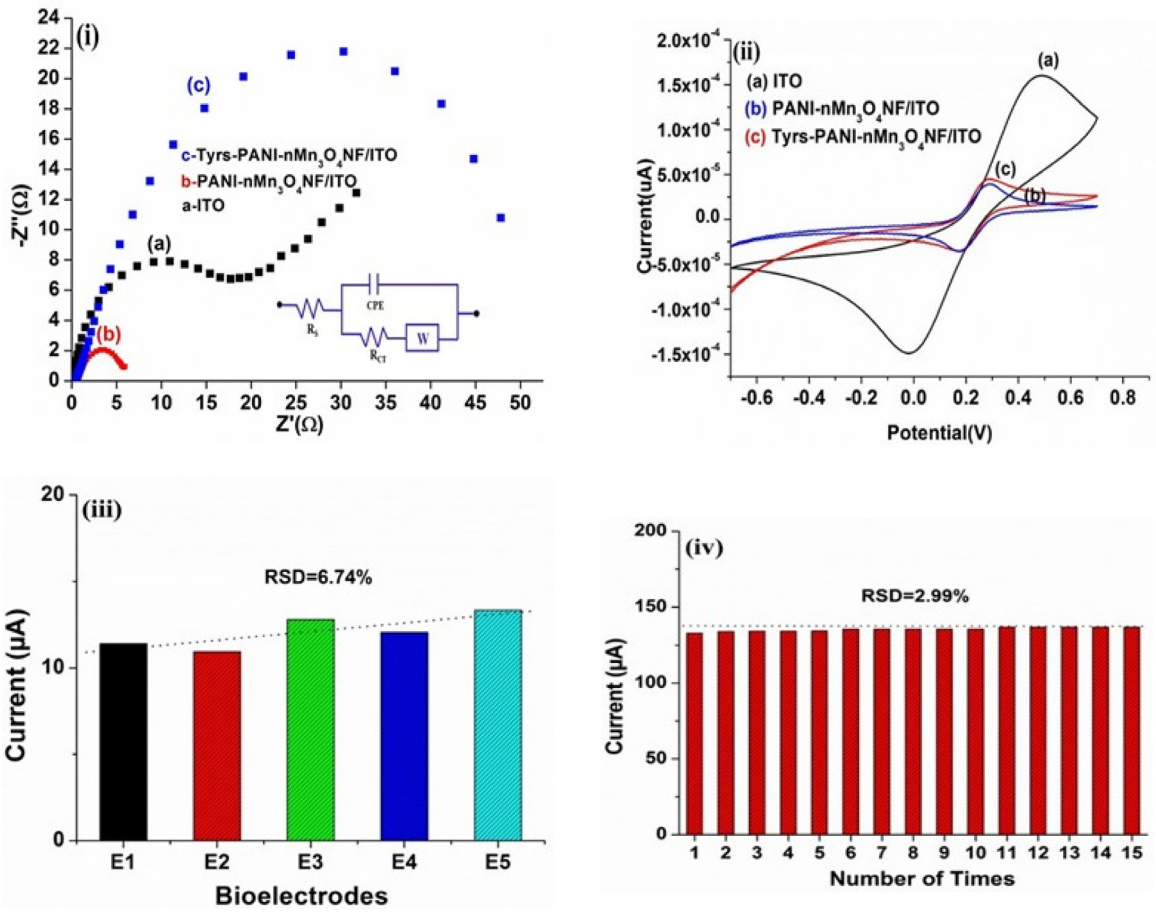

Fig. 8. (i) Electrochemical impedance spectroscopy (EIS) spectra of (a) ITO electrode, (b) PANI-nMn_3O_4/ITO electrode, and (c) Tyrs-PANI-nMn_3O_4/ITO bioelectrode in PBS (50 mM, pH 7.4) solution containing 5 mM $[Fe(CN)_6]^{3-/4-}$. (ii) The cyclic voltammogram of, (a) ITO electrode, (b) PANI-nMn_3O_4/ITO electrode, and (c)Tyrs-PANI-nMn_3O_4/ITO bioelectrode. (iii) The reproducibility of Tyrs-PANI-nMn_3O_4/ITO bioelectrode, and (iv) Repeatability of Tyrs-PANI-nMn_3O_4/ITO bioelectrode.

trode and electrolyte. The conductive nature of the nanocomposite, facilitates interfacial electron transfer from electrolyte towards the collector. Moreover, it appears that nanofibrous PANI suitably arranges the nMn_3O_4 on its surface and provides a better conformation for enzyme immobilization. Further, immobilization of Tyrs enzyme on PANI-nMn_3O_4NF/ITO surface, increases the R_{CT} value (curve c) due to presence of available functional groups (-NH_2 and −CHO) on the electrode surface. The enhancement of R_{CT} value (5.21 kΩ) for Tyrs-PANI-nMn_3O_4NF/ITO bioelectrode is due to the insulating nature of the Tyrs molecules that covalently bind with −NH_2 group of PANI *via* GA. The amount of immobilized enzyme has been optimized at 10.0 μL and the surface coverage of Tyrs-PANI-nMn_3O_4NF/ITO bioelectrode was calculated to be (62.76%), [3].

The electron transfer resistance can be translated into magnitude of current under the equilibrium (Io), heterogeneous electron-transfer rate constant (HET) and the time constant (τ) of the various electrodes have been calculated by the following Eqs. ((2)–(5)) [3].

$$R_{CT} = RT/nFI_0 \quad (2)$$

$$I_0 = nFAHET\,[S] \quad (3)$$

$$HET = RT/n^2F^2AR_{CT}\,[S] \quad (4)$$

$$\tau = R_{CT}C_{dl} \quad (5)$$

where R is gas constant, T is absolute temperature (K), F is Faraday constant, A is the electrode area (cm^2), [S] is the bulk concentration of redox probe ($mol\,cm^{-3}$), n is the number of transferred electrons per molecule of the redox probe and C_{dl} is the double layer capacitance. The HET value for ITO is found to be $0.014 \times 10^{-6}\,cm\,s^{-1}$. The HET value of PANI-$nMn_3O_4$NF/ITO electrode ($0.048 \times 10^{-6}\,cm\,s^{-1}$) is higher than that of Tyrs-PANI-nMn_3O_4NF/ITO bioelectrode ($0.0051 \times 10^{-6}\,cm\,s^{-1}$), indicating faster electron transfer among the redox couples. The Tyrs enzyme-immobilized electrode provides hindrance to the electron transfer resulting in a sluggish electron transfer. Further, high value of time constant (τ) for Tyrs-PANI-nMn_3O_4NF/ITO bioelectrode ($44.2\,cm\,s^{-1}$) shows slower diffusion rate ($8.4\,cm\,s^{-1}$) of $[Fe(CN)_6]^{3-/4-}$ ions at the solution/electrode interface.

The cyclic voltammetry (CV) studies have been conducted to investigate the electrochemical properties of the fabricated electrodes in the potential range of −0.7 to 0.7 V at a scan rate of 10 mV/s [Fig. 8(ii)]. After electropolymerization of PANI-nMn_3O_4 nanocomposite on ITO substrate, the oxidation current decreases (0.04 mA) [curve b] compared to that of the bare ITO electrode (1.6 mA) [curve a] revealing that the increased surface area of PANI-nMn_3O_4NF/ITO electrode may obstruct electron transfer. Interestingly, after immobilization of Tyrs enzyme on the surface of PANI-nMn_3O_4NF/ITO, the electrode shows increased current response (0.05 mA, curve c) compared to that of PANI-nMn_3O_4NF/ITO electrode (curve b). This may be attributed to the covalently bonded Tyrs molecules on the surface of PANI-nMn_3O_4NF/ITO providing a promising environment. The available active sites on Tyrs may be electrochemically activated in presence PANI-nMn_3O_4 NF that perhaps acts as a mediator resulting in accelerated electrons from redox reaction. The CV

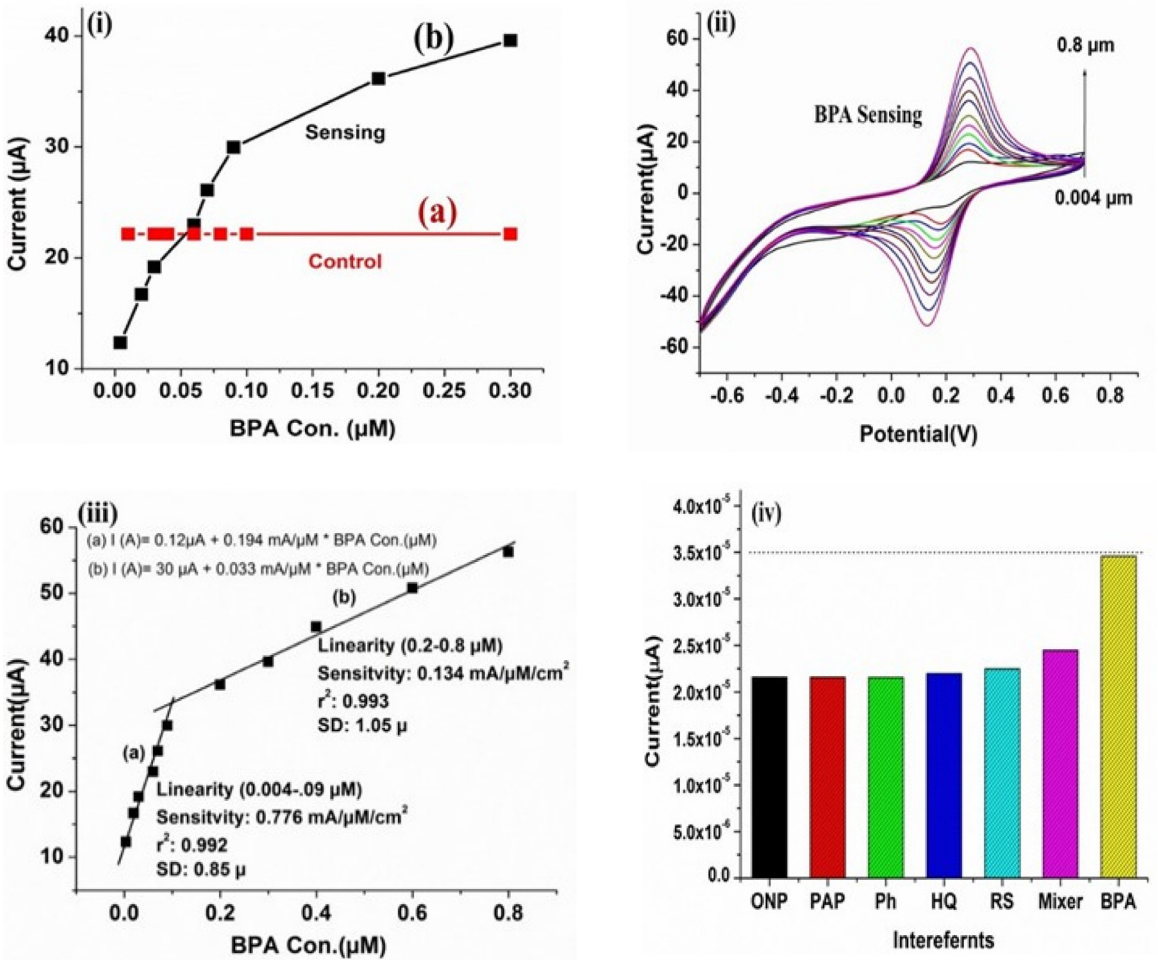

Fig. 9. (i) Control study of Tyrs-PANI-nMn$_3$O$_4$/ITO bioelectrode, (ii) Cyclic voltammogram of Tyrs-PANI-nMn$_3$O$_4$/ITO bioelectrode as a function of BPA concentration (0.004–0.8 μM) in PBS (50 mM, pH 7.4) solution containing 5 mM $[Fe(CN)_6]^{3-/4-}$. (iii) Calibration curve between oxidation current and BPA concentration (μM), and (iv) The selectivity of Tyrs-PANI-nMn$_3$O$_4$/ITO bioelectrode.

studies of Tyrs-PANI-nMn$_3$O$_4$NF/ITO bioelectrode have been conducted as a function of scan rate [Fig. S3]. The anodic (I_A) and cathodic (I_C) peak currents show linear variation with square root of the scan rate [inset in Fig. S3], suggesting that the reaction at the electrode is a quasi-reversible diffusion-controlled process. Both the peak currents are found to increase with increased scan rate (10–100 mV/s). The linear relationship of peak current versus square root of scan rate ($v^{1/2}$) in Tyrs-PANI-nMn$_3$O$_4$NF/ITO bioelectrode can be derived from the Nernst's equation due to presence of electro-active components in the interfacial region. The slope, intercept and correlation coefficient for the bioelectrode obey the following anodic (I_A) and cathodic (I_C) currents given in Eqs. ((6) and (7)):

$$I_A\,(\text{bioelectrode}) = 29.3\,\mu A + 1.60\times10^{-5}\left(A^2mV^{-1}s\right)^{1/2}\times \left[\text{Scanrate}\left(mVs^{-1}\right)\right]^{1/2};\ r^2 = 0.999 \quad (6)$$

$$I_C\,(\text{bioelectrode}) = -26.7\,\mu A - 0.76\times10^{-5}\left(A^2mV^{-1}s\right)^{1/2}\times \left[\text{Scanrate}\left(mVs^{-1}\right)\right]^{1/2};\ r^2 = 0.999 \quad (7)$$

The peak current is obtained by the Randles-Sevcik method, as described in Eq. (8)

$$I_p = \frac{n^2F^2CA\nu}{RT} \quad (8)$$

where I_p is the peak current (A), n is the number of electrons transferred in the redox process, F is the Faraday constant ($C\,mol^{-1}$), C is the concentration (mM), R is gas constant ($8.314\,J\,K^{-1}\,mol^{-1}$), υ is the scan rate (40 mV/s), A is the area of fabricated interface ($0.25\,cm^2$) and T is the absolute temperature (298 K). The diffusion coefficient of redox probe towards the sensing interface is calculated using Randles-Sevcik Eq. (8)

$$I_{p=2.69\times10^5 n^{3/2}AD^{1/2}Cv^{1/2}}$$

The diffusion coefficients are found to be $1.41\times10^{-6}\,cm^2/s$ and $2.21\times10^{-6}\,cm^2/s$ for PANI-nMn$_3$O$_4$NF/ITO electrode and Tyrs-PANI-nMn$_3$O$_4$NF/ITO bioelectrode, respectively. The higher diffusion after enzyme immobilization may be due to the formation of PANI-nMn$_3$O$_4$ fibrous film that accelerates the transport of electrons due to activation of enzyme active sites.

The reproducibility of Tyrs-PANI-nMn$_3$O$_4$NF/ITO bioelectrode [Fig. 8(iii)] was investigated at $0.01\times10^{-6}\,mol\,L^{-1}$ of BPA concentration. No significant change in the oxidation current was observed as was evident by relative standard deviation (RSD=6.74%). The stability of this bioelectrode was tested using repeated measurements under similar conditions. Even after 15 times of repeated

measurements, [Fig. 8(iv)], the Tyrs-PANI-nMn_3O_4NF/ITO bioelectrode showed identical response as is evident by low relative standard deviation (RSD=2.99%). The storage stability of the Tyrs-PANI-nMn_3O_4NF/ITO bioelectrode was checked for 8 weeks at an interval of one week. The decrease in the value of current was found to be about 10% up to 4 weeks after which the current value decreases to about 40% within 10 weeks.

3.3.1. Bisphenol A detection

Electrochemical response studies of Tyrs-PANI-nMn_3O_4NF/ITO biosensor were conducted using CV technique in presence of 50×10^{-3} mol L^{-1} PBS (pH 7.4, 0.9%NaCl) containing 5×10^{-3} mol L^{-1} $[Fe(CN)_6]^{3-/4-}$. The control experiments were conducted on PANI-nMn_3O_4NF/ITO electrode with and without Tyrs immobilization, using CV technique [Fig. 9(i)] by varying BPA concentrations. A small change observed in oxidation current (curve a) can be attributed to non-specific reaction with proteins on the sensor surface.

During detection of BPA, the bioelectrode was immersed in PBS solution containing various concentrations of BPA ($0.004–0.8 \times 10^{-6}$ mol L^{-1}). Due to the oxidation of BPA into 2, 2-bis (4-phenylquinone) propane in presence of Tyrs enzyme, two electrons are generated [Fig. 9 (ii)] that produce the current. It was observed that magnitude of the current gradually increased with increasing BPA concentration [Fig. 9(ii)]. In addition, this enhancement of electrochemical current may be due to well-arranged and homogenous network of bio-interface of the PANI-nMn_3O_4 nanofibrous film that provides a good path for electron transfer to current collector via manganese ion [35,36]. The three-dimensional nanofibrous morphology in PANI-nMn_3O_4NF/ITO electrode resulted in improved electronic and ionic transport due to uniform distribution and conductive nature of PANI-nMn_3O_4 NF. The detection time of this biosensor was to be 20 s indicating faster electron communication feature of PANI-nMn_3O_4 NF. The sensor calibration curve [Fig. 9(iii)] showed good linearity in a wide concentration range of $0.004–0.8 \times 10^{-6}$ mol L^{-1}. The current varied linearly with BPA concentration with a correlation coefficient of 0.993. The sensitivity of the fabricated biosensor calculated from the slope of calibration curve was found to be 0.776 mA μM^{-1} Lcm^{-2} and 0.134 mA μM^{-1} $L cm^{-2}$ for a lower concentration range ($0.004–0.09 \times 10^{-6}$ mol L^{-1}) and higher concentration ($0.2–0.8 \times 10^{-6}$ mol L^{-1}), respectively. The high sensitivity of this biosensor was due to high surface-to-volume ratio and conductive nature of PANI-nMn_3O_4 NF with better electron transportation from electrode surface to the electrolyte. This sensor could be used to detect minute amount of BPA (0.004×10^{-6} mol L^{-1}). The low value of the Michaelis–Menten constant (K_m) obtained [0.0075×10^{-6} mol L^{-1}] using Hanes plot reveals that PANI-nMn_3O_4 NF matrix facilitates increased enzyme activity due to improved conformation of Tyrs. The increased activity of Tyrs with covalent bonding indicates strong affinity between the BPA and the active site of Tyrs resulted in low K_m. The observed higher affinity of Tyrs-PANI-nMn_3O_4NF/ITO based biosensor can be attributed to favorable orientation of Tyrs and higher loading of Tyrs molecules. Table 1 contains characteristics of this sensor along with others reported in literature for BPA detection. The selectivity of Tyrs-PANI-nMn_3O_4NF/ITO bioelectrode [Fig. 9(iv)] was determined in presence of BPA (0.5×10^{-6} mol L^{-1}) concentration with normal concentration of interferent such as phenol (1.0×10^{-6} mol L^{-1}), ortho-nitrophenol (1.0×10^{-6} mol L^{-1}), para-aminophenol (0.8×10^{-3} mol L^{-1}), resorcinol (1.0×10^{-6} mol L^{-1}), hydroquinone (0.8×10^{-6} mol L^{-1}), and all mixers. The response of the Tyrs-PANI-nMn_3O_4NF/ITO bioelectrode was not significantly affected in the presence of interferents during BPA detection. The oxidation current value remained nearly same for all interferents with respect to BPA. The prepared biosensor was tested to detect

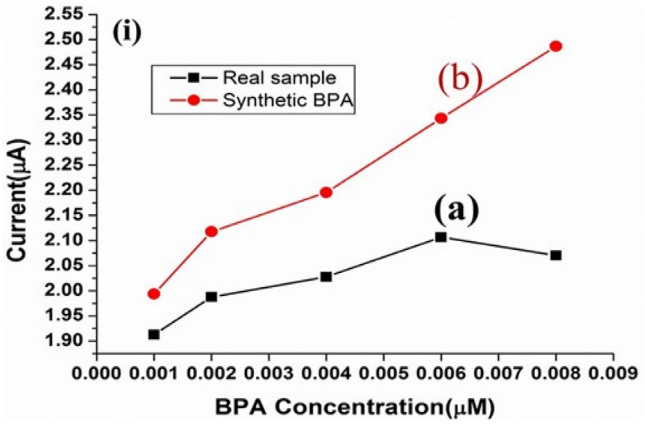

Fig. 10. (i) Cyclic voltammogram comparison study of Tyrs-PANI-nMn_3O_4/ITO bioelectrode as a function of synthetic BPA and real sample BPA concentration (0.001-0.008 μM) in PBS (50 mM, pH 7.4) solution containing 5 mM $[Fe(CN)_6]^{3-/4-}$.

BPA concentrations in real samples [Fig. 10 (i)]. In comparison to the standard BPA concentrations (curve b), the bioelectrode showed little difference at low real BPA concentrations other than higher concentration of BPA detection (curve a).

4. Conclusions

A cost-effective, reproducible, selective and highly sensitive PANI-nMn_3O_4 NF based biosensor platform has been demonstrated for BPA detection. We have electropolymerized *in-situ* PANI-nMn_3O_4 NF on an ITO substrate and used that for surface functionalization with Tyrs enzyme molecules via GA treatment. The fibrous surface of PANI-nMn_3O_4 NF performs a cross link with GA molecules for covalent immobilization of Tyrs enzyme resulting in improved sensing characteristics for monitoring BPA concentration. This biosensor is sensitive to 0.004×10^{-6} mol L^{-1} concentration of BPA due to the PANI-nMn_3O_4 NF biointerface, Mn^{2+} ion and cationic polyaniline that improves the charge transfer properties between electrode and electrolyte. The Tyrs-conjugated PANI-nMn_3O_4 NF provides suitable conduction path during oxidation of BPA leading to a fast electrochemical response (20s). This biosensor exhibits higher sensitivity (0.776 mA μM^{-1} Lcm^{-2}), low detection limit of 0.004×10^{-6} mol L^{-1}, lower K_m value 0.0075×10^{-6} mol L^{-1} with linear regression coefficient at 0.993 and a wide linear range of $0.004–0.8 \times 10^{-6}$ mol L^{-1}. The Tyrs-PANI-nMn_3O_4NF/ITO-based biosensor provides a suitable platform for excellent electrochemical sensing parameters due to the integration of PANI-nMn_3O_4NF and Tyrs via GA. The fabricated biointerface shows excellent sensitivity, selectivity, and good reproducibility and can be explored for monitoring other clinical substances such as low density lipoprotein, glucose, myoglobin etc.

Appendix A. Supplementary data

Supplementary data associated with this article can be found, in the online version, at http://dx.doi.org/10.1016/j.snb.2016.06.050.

References

[1] K.K. Reza, M.A. Ali, S. Srivastava, V.V. Agrawal, A.M. Biradar, Tyrosinase conjugated reduced graphene oxide based biointerface for bisphenol A sensor, Biosens. Bioelectron. 74 (2015) 644–651.
[2] L.N. Vandenberg, R. Hauser, M. Marcus, N. Olea, W.V. Welshons, Human exposure to bisphenol A (BPA), Reprod. Toxicol. 24 (2) (2007) 139–177 (Find This Artic Online.).
[3] N. Singh, K.K. Reza, M.A. Ali, V.V. Agrawal, A.M. Biradar, Self assembled DC sputtered nanostructured rutile TiO2 platform for bisphenol A detection, Biosens. Bioelectron. 68 (2015) 633–641.

[4] J.R. Roy, S. Chakraborty, T.R. Chakraborty, Estrogen-like endocrine disrupting chemicals affecting puberty in humans–a review, Med. Sci. Monit. 15 (2009) RA137–RA145.
[5] M. Regiart, S.V. Pereira, V.G. Spotorno, F.A. Bertolino, J. Raba, Food safety control of zeranol through voltammetric immunosensing on Au–Pt bimetallic nanoparticle surfaces, Analyst 139 (2014) 4702–4709.
[6] C. Nichols, X. Ding, G. Miranda-Carboni, S.A. Krum, Abstract 3192: the environmental estrogen bisphenol A (BPA) regulates mammary gland stem cells, Cancer Res. 74 (2014) 3192.
[7] P. Sohoni, C.R. Tyler, K. Hurd, J. Caunter, M. Hetheridge, T. Williams, C. Woods, M. Evans, R. Toy, M. Gargas, J.P. Sumpter, Reproductive effects of long-term exposure to bisphenol a in the fathead minnow (Pimephales promelas), Environ. Sci. Technol. 35 (2001) 2917–2925.
[8] G. Wang, Z. Chen, T. Bartell, X. Wang, Early life origins of metabolic syndrome: the role of environmental toxicants, Curr. Environ. Health Rep. 1 (2014) 78–89.
[9] D. Melzer, N.J. Osborne, W.E. Henley, R. Cipelli, A. Young, C. Money, P. McCormack, R. Luben, K.-T. Khaw, N.J. Wareham, T.S. Galloway, Urinary bisphenol A concentration and risk of future Coronary artery disease in apparently healthy men and women, Circulation 125 (2012) 1482–1490.
[10] A. Zafra, M. del Olmo, B. Suárez, E. Hontoria, A. Navalón, J.L. Víílchez, Gas chromatographic–mass spectrometric method for the determination of bisphenol A and its chlorinated derivatives in urban wastewater, Water Res. 37 (2003) 735–742.
[11] K. Inoue, Y. Yoshie, S. Kondo, Y. Yoshimura, H. Nakazawa, Determination of phenolic xenoestrogens in water by liquid chromatography with coulometric-array detection, J. Chromatogr. A 946 (2002) 291–294.
[12] K. Ma, T. Ekblad, M.K. Koerkamp, H. Kelderman, M. van Wijlen, A. Duarah, J. Yue, L. Zhang, M.V.-M. Wong, M.H. Lim, Contaminant detection in treated water using Optiqua's MiniLab™ biosensing system: a case study for bisphenol A, Int. J. Environ. Anal. Chem. 95 (2015) 366–378.
[13] Z. Xiao-hong, L. Lan-hua, X. Wei-qi, S. Bao-dong, S. Jian-wu, H. Miao, S. Han-chang, A reusable evanescent wave immunosensor for highly sensitive detection of bisphenol A in water samples, Sci. Rep. 4 (2014).
[14] J.-W. Park, S. Kurosawa, H. Aizawa, Y. Goda, M. Takai, K. Ishihara, Piezoelectric immunosensor for bisphenol A based on signal enhancing step with 2-methacrolyloxyethyl phosphorylcholine polymeric nanoparticle, Analyst 131 (2006) 155–162.
[15] D.K. Kim, P. Muralidharan, H.-W. Lee, R. Ruffo, Y. Yang, C.K. Chan, H. Peng, R.A. Huggins, Y. Cui, Spinel LiMn2O4 nanorods as lithium ion battery cathodes, Nano Lett. 8 (2008) 3948–3952.
[16] E. Hosono, T. Kudo, I. Honma, H. Matsuda, H. Zhou, Synthesis of single crystalline spinel LiMn2O4 nanowires for a lithium ion battery with high power density, Nano Lett. 9 (2009) 1045–1051.
[17] P. Li, C. Nan, Z. Wei, J. Lu, Q. Peng, Y. Li, Mn3O4 nanocrystals: facile synthesis, controlled assembly, and application, Chem. Mater. 22 (2010) 4232–4236.
[18] S. Fritsch, J. Sarrias, A. Rousset, G.U. Kulkarni, Low-temperature oxidation of Mn3O4 hausmannite, Mater. Res. Bull. 33 (1998) 1185–1194.
[19] Z. Weixin, W. Cheng, Z. Xiaoming, X. Yi, Q. Yitai, Low temperature synthesis of nanocrystalline Mn3O4 by a solvothermal method, Solid State Ion. 117 (1999) 331–335.
[20] P.Z. Si, D. Li, C.J. Choi, Y.B. Li, D.Y. Geng, Z.D. Zhang, Large coercivity and small exchange bias in Mn3O4/MnO nanoparticles, Solid State Commun. 142 (2007) 723–726.
[21] A. Vázquez-Olmos, R. Redón, G. Rodríguez-Gattorno, M. Esther Mata-Zamora, F. Morales-Leal, A.L. Fernández-Osorio, J.M. Saniger, One-step synthesis of Mn3O4 nanoparticles: structural and magnetic study, J. Colloid Interface Sci. 291 (2005) 175–180.
[22] K. Kamil Reza, N. Singh, S.K. Yadav, M.K. Singh, A.M. Biradar, Pearl shaped highly sensitive Mn3O4 nanocomposite interface for biosensor applications, Biosens. Bioelectron. 62 (2014) 47–51.
[23] Y. Chen, X.H. Wang, J. Li, J.L. Lu, F.S. Wang, Polyaniline for corrosion prevention of mild steel coupled with copper, Electrochim. Acta 52 (2007) 5392–5399.
[24] Y. Sun, J.A. Rogers, Inorganic semiconductors for flexible electronics, Adv. Mater. 19 (2007) 1897–1916.
[25] C. Dhand, S.K. Arya, S.P. Singh, B.P. Singh, M. Datta, B.D. Malhotra, Preparation of polyaniline/multiwalled carbon nanotube composite by novel electrophoretic route, Carbon 46 (2008) 1727–1735, http://dx.doi.org/10.1016/j.carbon.2008.07.028.
[26] X. Qin, S. Liu, W. Lu, H. Li, G. Chang, Y. Zhang, J. Tian, Y. Luo, A.M. Asiri, A.O. Al-Youbi, X. Sun, Submicrometre-scale polyaniline colloidal spheres: photopolymerization preparation using fluorescent carbon nitride dots as a photocatalyst, Catal. Sci. Technol. 2 (2012) 711–714, http://dx.doi.org/10.1039/C2CY00439A.
[27] G. Chang, Y. Luo, W. Lu, X. Qin, A.M. Asiri, A.O. Al-Youbi, X. Sun, Ag nanoparticles decorated polyaniline nanofibers: synthesis, characterization, and applications toward catalytic reduction of 4-nitrophenol and electrochemical detection of H2O2 and glucose, Catal. Sci. Technol. 2 (2012) 800–806, http://dx.doi.org/10.1039/C2CY00454B.
[28] S. Liu, L. Wang, Y. Luo, J. Tian, H. Li, X. Sun, Polyaniline nanofibres for fluorescent nucleic acid detection, Nanoscale 3 (2011) 967–969, http://dx.doi.org/10.1039/C0NR00873G.
[29] Z.W. Chen, J.K.L. Lai, C.H. Shek, Nucleation site and mechanism leading to growth of bulk-quantity Mn3O4 nanorods, Appl. Phys. Lett. 86 (2005) 181911, http://dx.doi.org/10.1063/1.1923753.
[30] H. Kavas, Z. Durmus, M. Şenel, S. Kazan, A. Baykal, M.S. Toprak, CTAB-Mn3O4 nanocomposites: synthesis, NMR and low temperature EPR studies, Polyhedron 29 (2010) 1375–1380, http://dx.doi.org/10.1016/j.poly.2009.12.034.
[31] Z. Zheng, Y. Du, Z. Wang, Q. Feng, C. Wang, Pt/graphene–CNTs nanocomposite based electrochemical sensors for the determination of endocrine disruptor bisphenol A in thermal printing papers, Analyst 138 (2012) 693–701, http://dx.doi.org/10.1039/C2AN36569C.
[32] A.I. Inamdar, Y.S. Kim, J.S. Sohn, H. Im, H. Kim, D.-Y. Kim, R.S. Kalubarme, C.H. Park, Supercapacitive characteristics of electrodeposited polyaniline thin films grown on indium doped tin oxide substrates, J. Korean Phys. Soc. 59 (2011) 145–149.
[33] D.P. Dubal, D.S. Dhawale, R.R. Salunkhe, S.M. Pawar, C.D. Lokhande, A novel chemical synthesis and characterization of Mn3O4 thin films for supercapacitor application, Appl. Surf. Sci. 256 (2010) 4411–4416, http://dx.doi.org/10.1016/j.apsusc.2009.12.057.
[34] B.-Y. Chang, S.-M. Park, Integrated description of electrode/electrolyte interfaces based on equivalent circuits and its verification using impedance measurements, Anal. Chem. 78 (2006) 1052–1060, http://dx.doi.org/10.1021/ac051641l.
[35] H. Xia, Y.S. Meng, X. Li, G. Yuan, C. Cui, Porous manganese oxide generated from lithiation/delithiation with improved electrochemical oxidation for supercapacitors, J. Mater. Chem. 21 (2011) 15521–15526, http://dx.doi.org/10.1039/C1JM12767E.
[36] H. Jiang, T. Zhao, J. Ma, C. Yan, C. Li, Ultrafine manganese dioxide nanowire network for high-performance supercapacitors, Chem. Commun. 47 (2011) 1264–1266, http://dx.doi.org/10.1039/C0CC04134C.
[37] D.C. Apodaca, R.B. Pernites, R. Ponnapati, F.R. Del Mundo, R.C. Advincula, Electropolymerized molecularly imprinted polymer film: EIS sensing of bisphenol A, Macromolecules 44 (2011) 6669–6682, http://dx.doi.org/10.1021/ma2010525.
[38] Q. Li, H. Li, G.-F. Du, Z.-H. Xu, Electrochemical detection of bisphenol A mediated by [Ru(bpy)3]2+ on an ITO electrode, J. Hazard. Mater. 180 (2010) 703–709, http://dx.doi.org/10.1016/j.jhazmat.2010.04.094.
[39] H. Yin, Y. Zhou, J. Xu, S. Ai, L. Cui, L. Zhu, Amperometric biosensor based on tyrosinase immobilized onto multiwalled carbon nanotubes-cobalt phthalocyanine-silk fibroin film and its application to determine bisphenol A, Anal. Chim. Acta. 659 (2010) 144–150, http://dx.doi.org/10.1016/j.aca.2009.11.051.
[40] M. Portaccio, D. Di Tuoro, F. Arduini, M. Lepore, D.G. Mita, N. Diano, L. Mita, D. Moscone, A thionine-modified carbon paste amperometric biosensor for catechol and bisphenol A determination, Biosens. Bioelectron. 25 (2010) 2003–2008, http://dx.doi.org/10.1016/j.bios.2010.01.025.
[41] J. Huang, X. Zhang, S. Liu, Q. Lin, X. He, X. Xing, W. Lian, Electrochemical sensor for bisphenol A detection based on molecularly imprinted polymers and gold nanoparticles, J. Appl. Electrochem. 41 (2011) 1323–1328, http://dx.doi.org/10.1007/s10800-011-0350-8.

Biographies

Nawab Singh is doing PhD at the Indian Institute of Technology Hyderabad Telangana, India, in the Department of Biomedical Engineering. He received his MSc from Chaudhary Charan Singh University, Meerut, India (2010). Nawab's research interests are in micro/nano fabrication of functional nanomaterials, self and directed assembly, microfluidics based biochips for biomolecules detection, polymer thin-films, biomaterials for biosensing application. He has published 4 papers in peer-reviewed journals.

Md. Azahar Ali received his PhD degree from Biomedical Engineering Department at Indian Institute of Technology Hyderabad, India in collaboration with Biomedical Instrumentation Section at National Physical Laboratory, New Delhi, India. He also received his Master of Technology degree from Department of Electronics Engineering, Tezpur University, Assam in 2009. Currently, he is doing Post-Doctoral Associate at Electrical and Computer Engineering, Iowa State University, USA. He is actively engaged in the area of microfluidic based multiplex biochips for biomolecules detection.

Kali Suresh is doing Project Officer at the Indian Institute of Technology Hyderabad Telangana, India, in the Department of Chemical Engineering. He received his MSc from National Institute of Technology Warangal, Telangana, India (2010). Kali research interests are in Carbon based hierarchical structures. He has published 2 papers in peer-reviewed journals.

Ved Varun Agrawal earned his PhD degree from the Jawaharlal Nehru Center for Advanced Scientific Research in 2008. He now works as a Scientist in the Department of Science & Technology of Biomolecular Electronics, Biomedical Instrumentation Section at National Physical Laboratory (CSIR), New Delhi, India. His current research focuses on utilizing the properties of nanomaterials to improve biosensing characteristics.

Prabhakar Rai is working as INSPIRE Faculty in the Department of Chemical Engineering at Indian Institute of Technology Kanpur, India. He received his Ph.D. degree in Informatic Electronics Materials Engineering in 2012 from Chonbuk National University, South Korea. He was appointed as Research Professor in the Department of Materials Science and Engineering at Korea University, South Korea in 2013. His

research is mainly focused on synthesis of nanoscale metals and metal oxides for energy and chemical sensing applications.

Ashutosh Sharma is a Chair Professor in Chemical Engineering at the Indian Institute of Technology at Kanpur (IITK). Ashutosh received his Ph.D. from the State University of New York at Buffalo (1987), MS from the Pennsylvania State University (1984) and B. Tech. from IITK(1982).Ashutosh's research interests are in soft functional interfaces, micro/nano-mechanics of confined soft matter, self-organized patterning, soft nanofabrication, colloid and interfacial engineering, carbon nanocomposites and carbon MEMS/NEMS in energy, health and environmental applications, and membranes. He is currently Secretary to the Government of India, Department of Science and Technology starting January 2015

B.D. Malhotra received his Ph.D. degree from the University of Delhi, Delhi, India in 1980. He has published more than 270 papers in peer-reviewed journals, filed 10 patents, and edited/co-edited books on biosensors and polymer electronics. After his stint as Chief Scientist and Head of the DST Centre on Biomolecular Electronics at the CSIR-National Physical Laboratory, New Delhi, India, he moved to Delhi Technological University (DTU), India. He has nearly 30 years of research experience in the field of biomolecular electronics and has guided 25 Ph.D. students to date. His current activities include biosensors, nanobiomaterials, conducting polymers, and ordered molecular assemblies including Langmuir–Blodgett films and self-assembled monolayers among others. Dr. Malhotra is a Fellow of the Indian National Science Academy (INSA), the National Academy of Sciences, India (NASI) and an Academician of the Asia- Pacific Academy of Materials (APAM).

Renu John is currently an Associate Professor and Head of the Department of Biomedical Engineering, Indian Institute of Technology Hyderabad. He received his PhD degree from Indian Institute of Technology Delhi in 2006. He carried out his post-doctoral research at Fitzpatrick center for Photonics, Duke University, Durham, NC, USA and Biophotonics Imaging Laboratory, University of Illinois, Urbana-Champaign, USA. His research interests include Nano-Biophotonics, non-invasive NIR bio-imaging, 3-D phase microscopy Optical coherence tomography (OCT), Chemical and optical Biosensors.